Distinct immune cell dynamics mark adverse events and antibody responses of SARS-CoV-2 mRNA vaccine

Tomohiro Takano
National Institute of Infectious Diseases
Miwa Morikawa
Tokyo Shinagawa Hospital
Yu Adachi
National Institute of Infectious Diseases
Kiyomi Kabasawa
Tokyo Shinagawa Hospital
Nicolas Sax
KOTAI Biotechnologies, Inc.
Saya Moriyama
National Institute of Infectious Diseases
Lin Sun
National Institute of Infectious Diseases
Masanori Isogawa
National Institute of Infectious Diseases
Ayae Nishiyama
National Institute of Infectious Diseases
Taishi Onodera
National Institute of Infectious Diseases
Kazutaka Terahara
National Institute of Infectious Diseases
Keisuke Tonouchi
National Institute of Infectious Diseases
Masashi Nishimura
Tokyo Shinagawa Hospital
Kentaro Tomii
AIST https://orcid.org/0000-0002-4567-4768
Kazuo Yamashita
KOTAI Biotechnologies, Inc.
Takayuki Matsumura (matt@niid.go.jp)

National Institute of Infectious Diseases https://orcid.org/0000-0003-1760-3484
Masaharu Shinkai
Tokyo Shinagawa Hospital
Yoshimasa Takahashi
National Institute of Infectious Diseases https://orcid.org/0000-0001-6342-4087

Article

Keywords: biomarkers, SARS-CoV-2, mRNA vaccine, immune cell dynamics

Posted Date: September 17th, 2021

DOI: https://doi.org/10.21203/rs.3.rs-916246/v1

Abstract

Pfizer/BioNTec BNT162b2 mRNA vaccine robustly elicits neutralizing antibodies against SARS-CoV-2 in clinical trials and real-world settings. However, booster vaccinations are frequently associated with self-limited adverse events. Here, by applying a high-dimensional immune profiling approach to peripheral blood, we linked early vaccine-induced immune dynamics with adverse events and neutralizing antibody responses. The dynamics of two dendritic cell subsets (DC3s and AS-DCs) were identified as the specific correlates for adverse events; the combination of these cell dynamics stratified the vaccinees with severe reactogenicity, while the stratification did not affect the neutralizing antibody titers. Furthermore, the NKT-like cell dynamics that correlated with adverse events and antibody titers were accounted for distinct magnitudes of both events by sex and age. The identified immune correlates for adverse events and antibody responses may pave the way for a rational vaccine strategy for reducing the reactogenicity of mRNA vaccines without compromising the immunogenicity.

Main

The Pfizer/BioNTec BNT162b2 mRNA vaccine in a two-dose setting induces robust neutralizing antibodies against SARS-CoV-2 with 95% efficacy in preventing severe COVID-19[1]. However, the vaccine frequently triggers adverse events that are more exaggerated following booster vaccination. The mechanistic insights into these adverse events are required to reduce their harm while maintaining immunogenicity. To this end, it is crucial to identify the immune cell subsets and pathways that are selectively linked to adverse events and not to the neutralizing antibody responses, and vice versa. In this study, 92 healthcare workers who received an mRNA vaccine were enrolled.

As summarized in Extended Data Fig. 1, the median age of the 92 vaccinees was 39 years (interquartile range [IQR]: 28–50), ranging from 22 to 72 years, and 29 of 92 vaccinees (32%) were male. There was no significant difference in median age between males (n = 29, median: 40, IQR: 28–60) and females (n = 63, median: 39, IQR: 29–46), but the maximum of the IQR was higher in males. Males (n = 29, median: 23.9, IQR: 21.6–24.7) had a significantly higher BMI than females (n = 58, median: 20.9, IQR: 19.4–23.4). None of the participants had prior histories of COVID-19 diagnosis or anti-nucleocapsid antibodies in pre- or post-vaccinated plasma.

Results

Immune profiling of BNT162b2 vaccination reveals dramatic immunological changes after secondary vaccination

To elucidate the early vaccine-induced immune responses, peripheral blood at day 1 after primary and secondary vaccination was subjected to high-dimensional flow cytometric phenotyping, which quantifies 18 immune cells at high resolution (Extended Data Fig.2). Adverse events (local and systemic symptoms) were evaluated as symptom scores based on a self-reported questionnaire. The same criteria used for the

clinical trial of the BNT162b2 mRNA vaccine was applied in this study[1]. IgG against spike protein receptor-binding domain (RBD) and neutralizing (NT) antibodies in plasma were quantified at the indicated time points (Fig. 1a). The vaccinees who received the first dose were seropositive for RBD IgG (100%) and NT titers (74%) at three weeks post-vaccination, and the secondary vaccination further boosted the magnitudes of antibody titers to the levels in convalescent plasma from those who had recovered from severe COVID-19 (Fig. 1b,c)[2]. A more dramatic increase in NT titers relative to RBD IgG titers resulted in a significant elevation of the neutralizing potency index (NPI; NT activity per RBD IgG) (Fig. 1d), an antibody parameter correlating with affinity maturation[2].

Consistent with previous studies[1,3-8], both the local and systemic symptom scores increased 1.4- and 3.8-fold after secondary vaccination, respectively, relative to those after primary vaccination (Fig. 1e). More prominent adverse events were represented by higher incidence and elevated grades of systemic symptoms, such as fever, fatigue, headache, and chills after the secondary vaccination (Fig. 1f,g). The frequencies of the adverse events in this study were slightly higher than those in the original trial[1]; for example, fever (28% vs. 16%) and fatigue (72% vs. 59%), possibly reflecting younger median age (39 vs. 52 on average) and higher female ratios (68% vs. 49%) in the present study. Those who had severe local symptoms after primary vaccination tended to suffer from local symptoms again after secondary vaccination (Fig. 1h), whereas no significant correlation was noted for systemic symptoms between primary and secondary vaccination (Fig. 1i). The dissociation between the primary and secondary response suggests the possible involvement of immunological memory in exaggerating the systemic symptoms, which include not only memory T and B lymphocytes[9-13], but also myeloid cells[14,15].

To dissect immune cell dynamics behind adverse events and antibody responses, high-dimensional flow cytometric phenotyping was performed using the indicated markers and gating strategies (Extended Data Fig. 2). The frequency of each cell subset was quantified as a percentage of $CD45^+$ cells (Extended Data Fig. 3), and then the fold increases or decreases from pre- to post-vaccination were calculated and defined as dynamics hereafter. Uniform manifold approximation and projection (UMAP) was applied to visualize the trajectory of vaccine-induced dynamics of 18 cells following primary and secondary vaccinations (Fig. 1j). Pre-vaccination samples (days 0 and 21) merged with each other and revealed the baseline landscape based on 18 cell frequencies in the UMAP space. Of note, post-vaccination samples following primary (day 1) and secondary (day 22) vaccinations showed distinct distributions from the rest. The samples slightly shifted to the lower left in the primary responses, but shifted away from the pre-vaccination space to the lower right space in the secondary responses. The distinct trajectories and clustering obtained using UMAP between the primary and secondary vaccinations are likely independent of age, sex, and BMI (Extended Data Fig. 4), as these parameters failed to define the clusters revealed after vaccinations. Thus, the UMAP results visualized the profound and distinct dynamics of immune cells during secondary responses.

Early immune dynamics are linked to neutralizing antibody response

The possible links between these immune cell dynamics and antibody responses were evaluated during the primary (Fig. 2a) and secondary (Fig. 2b) responses. The dynamics of $CD4^+$ T cells after primary vaccination were inversely correlated with primary RBD IgG titers (Fig. 2a), but this correlation was not extended to functional NT parameters (Fig. 2a). Following secondary vaccination, negative correlations were found between NT titers and dynamics of four cell populations ($CD16^+$ NK cells, $CD56^{high}$ NK cells, NKT-like cells, and non-classical monocytes) (Fig. 2b-f), indicating that vaccinees who showed reduction in these cells had higher NT titers. It should be noted that NK and NKT-like cells decreased in frequency in >70% of the vaccinees in response to the secondary vaccination, probably reflecting the rapid recruitment of these cell subsets into inflammatory sites, as previously observed[16,17].

Monocytes are commonly identified as an immune correlate for antibody responses following influenza inactivated vaccines and COVID-19 mRNA vaccines[14,15,18]. In our study, the vaccinees with more profound reductions in non-classical monocytes mounted higher amounts of NT (Fig. 2f). Likewise, those who had reduced numbers of NK subsets following vaccination produced greater amounts of NT (Fig. 2c,d), similar to previous findings in influenza vaccinees[18]. Overall, the cellular subsets identified by our immune profiling approach overlapped with those from the systems vaccinology approach. An additional identification of NKT-like cell dynamics as an immune correlate for antibodies suggests greater sensitivity of our immune profiling analysis.

The possible regulatory cytokines and chemokines in the identified cell dynamics were assessed by quantifying the concentrations of multiple cytokines and chemokines in the plasma (Extended Data Fig. 5). Activated NK subsets and NKT-like cells rapidly produce IFN-γ. Indeed, the levels of IP-10, MCP-1, and MIG, all of which are IFN-γ inducible chemokines, were higher following secondary vaccination with inverse correlation to the dynamics of NK and NKT-like cells (Fig. 2g). Furthermore, these chemokines positively correlated with the NT titers. Together, these data suggest that rapid NK migration into inflammatory sites leads to the production of IFN-γ and its inducible chemokines, and that the NK-IFN-γ pathway correlates with and is predictive of the subsequent magnitude of antibody responses, which is consistent with previous results using systems vaccinology approaches[14,18].

Correlations between adverse events and neutralizing antibodies

The correlations between antibody titers (RBD IgG) and adverse events remain controversial[3-7]. Here, we addressed this point by quantifying the functional NT titers in our cohort. We found a significant correlation between pain at the injection site and RBD IgG/NT titers (Fig. 3a), but the sum of local symptoms was linked to the NT titers only (Fig. 3a). The vaccinees were then stratified into three groups based on their symptom scores, and antibody titers were compared among the groups with different severity of symptoms (Fig. 3b-e). After the primary vaccination, NT titers, but not RBD IgG, were >5-fold higher in the vaccinees with severe local symptoms (>3) compared to those without symptoms (Fig. 3b,c). However, the antibody titers following the primary vaccination were not correlated with the severity of systemic symptoms (Fig. 3d,e), suggesting that primary antibody responses are largely governed by local immune responses.

Conversely, the NT titers following the secondary vaccination correlated with multiple systemic symptoms but not with local symptoms (Fig. 3f-j). A comparative analysis revealed a 2.5-fold increase in NT titers in those who suffered from severe systemic symptoms, while RBD IgG titers remained unchanged (Fig. 3i,j). Thus, these results unveiled the dose- and symptom-dependent correlations between NT titers and symptoms, highlighting the links between local symptoms and primary NT titers and those between systemic symptoms and secondary NT titers. Similar to NT titers in Fig. 2g, IFN-γ inducible chemokines positively correlated with the severity of systemic symptoms following the secondary vaccination (Fig. 3k).

Immune cell dynamics are linked to adverse events

Next, we attempted to identify the cell dynamics that are more tightly linked to adverse events than to antibody responses as such information is important for attenuating adverse event without compromising immunogenicity of the vaccine. To identify such immune events, correlation analyses were performed between the cell dynamics and local/systemic symptoms during the primary (Extended Data Fig. 6) and secondary responses (Fig. 4a,b). No significant correlations were observed between the sum of symptoms and the cellular dynamics during the primary response (Extended Data Fig. 6), but three cellular populations correlated with the sum of systemic but not local symptoms during the secondary responses (Fig. 4a,b). Among them, the dynamics of NKT-like cells after second vaccination were also found to negatively correlate with NT responses (Fig. 4c); on the other hand, the dynamics of $CD11c^-$ AS-DCs and DC3s after second vaccination were negatively correlated with the severity of systemic symptoms (but not with NT responses) in rather specific way (Fig. 4d,e).

We next evaluated the discriminative value of the identified cellular dynamics for systemic symptoms and antibody responses following secondary vaccination. First, three cell populations (NKT-like, $CD11c^-$ AS-DC, and DC3) were selected (Fig. 5a) and combined into a Z-score to visualize the correlation with NT titers (Fig. 5b) and systemic symptom scores (Fig. 5c). The combined parameter showed a stronger correlation with systemic symptom scores than individual parameters (Fig. 5c; $r = -0.34$ versus $r = -0.30 \sim -0.22$ in Fig. 4c-e) and failed to correlate with NT titers. To test the utility of these three parameters for stratifying the vaccinees with severe reactogenicity, the vaccinees were separated into matched groups that were positive (i.e., the post/pre ratios were below the median of the cohort) for all three parameters, and non-matched groups that were negative (i.e., the post/pre ratios were above the median of the cohort) for the three parameters. Stratification by the three parameters slightly increased the NT titers in the matched group with statistically insignificant level (Fig. 5d), but the matched group led to a significant 2.3-fold increase in systemic symptoms (Fig. 5e).

Next, the two parameters ($CD11c^-$ AS-DC and DC3) linked to the adverse events but not to antibody titers were combined to increase the specificity for those who had severe symptoms without affecting the NT titers (Fig. 5f). The combined Z-score did not correlate with NT titers (Fig. 5g), but correlated with systemic symptom scores (Fig. 5h). Also, the stratification by the two selected parameters left the NT

titers unchanged in the matched group (Fig. 5i), but the matched group showed increased systemic symptom scores by 1.8-fold compared to the scores of the non-matched group (Fig. 5j).

Effects of sex and age on immune dynamics

Females typically develop higher antibody responses and experience more adverse events following SARS-CoV-2 mRNA vaccination than males[6,19,20]. Consistently, the females in our cohort displayed higher levels of RBD IgG (1.4-fold) and NT (1.3-fold) antibodies than males following the secondary vaccination (Fig. 6a,b), although the differences in NT titers were not statistically significant. The females also experienced 1.8-fold more severe adverse events than males (Fig. 6c). To identify the early immune dynamics behind the sex difference, we compared the cellular dynamics that were identified as the cellular correlates of NT titers and systemic symptoms between males and females. Three NT-specific parameters (the dynamics of $CD16^{+}$ NK cells, $CD56^{high}$ NK cells, and non-classical monocytes) and two symptom-specific parameters (the dynamics of $CD11c^{-}$ AS-DCs and DC3s) were comparable between males and females (Fig. 6d); however, we found significantly lower post/pre ratios of NKT-like cells in females. We also observed significantly higher levels of IP-10 in plasma from females (Fig. 6e). Of note, NKT-like cell frequency was the only parameter shared with NT titers and systemic symptoms (Fig. 5). Collectively, females decreased the numbers of NKT-like cells more profoundly following the secondary vaccination; potentially explaining the higher antibody titers and adverse events compared to males.

Age is another parameter inversely associated with antibody responses and adverse events caused by COVID-19 mRNA vaccines[5,7,19,20]. In line with this, age was negatively correlated with NT titers and systemic symptom scores in our cohort (Fig. 6f-h). The possible cell dynamics behind the age-associated hypo-responses were determined using a correlation matrix (Fig. 6i), revealing significant correlations with three cell subsets ($CD16^{+}$ NK cells, NKT-like cells, and non-classical monocytes) (Fig. 6j-l) and a negative correlation with IFN–inducible chemokines (Fig. 6i).

Discussion

By profiling 18 immune cell dynamics at day 1 post-vaccination, we identified six cellular dynamics that correlated with the adverse events as well as the induction of neutralizing antibodies at later time points. These include the innate immune cell dynamics that have been suggested as the correlates of vaccine-induced antibody responses via the systems vaccinology approach[14,15,18]. This study identifies the reduction of NKT-like cells in peripheral blood as an additional correlate of high antibody titers and severity of systemic symptoms; these findings accounted for higher magnitudes of both events in females and lower magnitudes in the elderly. The most striking finding of this study was to identify the reduction of DC3s and $CD11c^{-}$ AS-DCs as the specific correlates for adverse events, and the combination of two parameters successfully predicted the vaccinees who suffered from adverse effects. Thus, the dynamics of these DC subsets could be useful as specific correlates for adverse events.

A key question is whether the cell dynamics of two DC subsets have any causal relationship with exaggerated systemic adverse events. Intramuscular vaccination induces local inflammation at the injection site and recruits multiple cell subsets, including DCs, into the tissue or draining lymph nodes[21,22], resulting in a decrease in these cells from circulation in response to the secondary vaccination. Both DC subsets are newly classified subsets via high-resolution single cell analysis[23–29], the biological functions of these DC subsets remain largely unknown. DC3s are considered a distinct subset that is specialized to produce pro-inflammatory cytokines (TNF, IL-1β, IL-6, IL-12, IL-23, etc.)[23]. Some of these cytokines possess pyrogenic effects and differentiate antigen-stimulated T cells into Th1 or Th17 subsets to accelerate inflammation[30 – 33], possibly contributing to the exacerbated adverse events. On the other hand, functional analysis is still limited in $CD11c^-$ AS-DCs, and how this DC subset links with adverse events requires further investigation.

No significant correlations in symptomatic scores between primary and secondary vaccinations imply the presence of unknown factors that emerge by primary vaccination and worsen the systemic symptoms. Moreover, the factors likely regulate DC3 and $CD11c^-$ AS-DC dynamics via direct or indirect ways upon the secondary vaccination. In this context, exaggerated adverse events in vaccinees with previous infection histories are noteworthy[8,34] and imply the involvement of immunological memory for worsening adverse events. In this scenario, such symptom-enhancing memory responses can initially be primed by SARS-CoV-2 antigens without the formulation of mRNA vaccines. This reduces the possible involvement of chemical compounds, such as polyethylene glycol, to generate the symptom-enhancing memory. Moreover, the memory responses are unlikely to wane in a short period of time, since symptom enhancement is observed in individuals who have experienced a previous infection greater than 6 months prior[8]. The identification of the symptom-enhancing memory is pivotal for mechanistic understanding of vaccine-induced adverse events and accelerates the development of vaccine strategy for reducing the reactogenicity without comprising the immunogenicity.

Methods

Study design

Healthcare workers without a prior history of SARS-CoV-2 infection at Tokyo-Shinagawa Hospital were enrolled. All participants were confirmed to be seronegative (< 0.1) for nucleocapsid antibodies by Elecsys Anti-SARS-CoV-2 (Roche) at enrollment. All volunteers provided written informed consent prior to enrollment. The participants received two doses of the Pfizer/BioNTech BNT162b2 vaccine. Secondary vaccination was conducted on day 21 after the primary vaccination. Blood samples were collected at five time points for longitudinal analyses: day 0 (the day of first vaccination), day 1, day 21 (the day of second vaccination), day 22, and day 47–51. The following information was collected for each participant: sex, age, body mass index (BMI), pre-existing medical conditions (hypertension, diabetes mellitus, and dyslipidemia), and history of PCR-confirmed SARS-CoV-2 infection. All studies were approved by the Institutional Review Board of the National Institute of National Institute of Infectious

Diseases and Tokyo Shinagawa Hospital (Permit numbers: 1292 and 20-A-33). This study was performed in accordance with the principles of the Declaration of Helsinki.

Sample processing and cell isolation.

Blood samples were collected in Vacutainer CPT tubes (BD Biosciences), and peripheral blood mononuclear cells (PBMCs) and plasma samples were isolated via centrifugation at 1800 × *g* for 20 min. PBMCs and plasma samples were separated by centrifugation at 300 × *g* for 15 min. Plasma samples were isolated via additional centrifugation at 800 × *g* for 15 min and stored at -80 °C until further analysis. For ELISA and pseudotyped virus-neutralizing assays, plasma samples were used after heat-inactivation at 56 °C for 30 min. For cytokine/chemokine quantification, plasma samples were used immediately after thawing at room temperature. PBMCs were centrifuged at 300 × *g* for 10 min and washed twice with PBS (FUJIFILM Wako Chemicals). PBMCs were used immediately after isolation for analysis of MDSCs (e-MDSCs, M-MDSCs, and PMN-MDSCs), or cryopreserved at -135 °C using CELLBANKER 1 plus (ZENOGEN PHARMA) for additional analysis.

Adverse events questionnaire

All participants completed two questionnaires on vaccine-related adverse events that occurred during days 1–7 (primary vaccination-related adverse events) and days 22–29 (secondary vaccination-related adverse events). Questionnaires asked about the presence of three local symptoms (pain, redness, and swelling) and eight systemic symptoms (fever, fatigue, headache, chills, vomiting, diarrhea, muscle pain, and joint pain), and the symptom severities were evaluated on five grades (grade 0–4, see Supplemental Information S1). The criteria used for the clinical trial of the BNT162b2 mRNA vaccine were applied[1]. Local 3 symptom severity scores and systemic 8 symptom severity scores were summed for the total local symptom severity score and total systemic symptom severity score, respectively.

ELISA

The human codon-optimized nucleotide sequence encoding the spike protein of the SARS-CoV-2 isolate (GenBank: MN995567) was commercially synthesized (Eurofinsgenomics). RBD (amino acids: 331-529) with the signal peptide (amino acids: 1-20; MIHSVFLLMFLLTPTESYVD) with a C-terminal histidine tag was cloned into the mammalian expression vector pCAGGS. Recombinant proteins were produced using Expi293F cells according to the manufacturer's instructions (Thermo Fisher Scientific). Expi293F cells were maintained in Expi293 expression medium (Thermo Fisher Scientific). The supernatant from transfected cells was harvested on day 5 post-transfection, and recombinant proteins were purified using Ni-NTA agarose (QIAGEN).

A recombinant reference monoclonal antibody (CR3022) was prepared as previously described[35,36]. Briefly, the V_H/V_L genes of CR3022 were cloned into expression vectors with human IgG1 heavy chain and kappa light chain. Pairs of heavy and light chain vectors were transfected into Expi293F cells according

to the manufacturer's instructions. Thereafter, CR3022 was purified from the culture supernatant using a protein G column (Thermo Fisher Scientific) and dialyzed with PBS.

F96 Maxisorp Nunc-Immuno plates (Thermo Fisher Scientific) were coated with 2 μg/mL of RBD protein overnight at 4 °C. After washing with PBS, the plates were blocked with 1% bovine serum albumin (BSA) in PBS for 1.5 h at room temperature. Heat-inactivated plasma and monoclonal antibodies were serially diluted in PBS containing 1% BSA and 0.1% Tween-20 (eight 4-fold serial dilutions starting at 1:20 dilution for plasma, and eight 4-fold serial dilutions starting at 1 μg/mL for monoclonal antibody), then incubated overnight at 4 °C. The following day, plates were washed with PBS containing 0.05% Tween-20. HRP-conjugated goat anti-human IgG (Southern Biotech) was diluted in Can Get Signal Immunoreaction Enhancer Solution 2 (TOYOBO) and incubated for 1.5 h at room temperature. After washing the plates with PBS containing 0.05% Tween-20 and PBS, HRP-activity was visualized by the addition of OPD substrate (Sigma), and OD490 was measured using an Epoch2 microplate reader (Biotek) and iMark microplate reader (Bio-Rad). IgG titers were quantified using CR3022 as a reference antibody in each plate.

RBD IgG titers of COVID-19 convalescent patients were partially referred from data used in Figure 1C of a previous publication[2]. The criteria for data selection were (1) time points 23–64 days after symptom onset, and (2) severe symptom severity defined by the WHO.

Pseudotyped virus neutralization assay

VSV pseudotyped virus bearing SARS-CoV-2 spike protein was generated as described previously[37]. Briefly, the cDNA of the SARS-CoV-2 spike protein was synthesized (Integrated DNA Technologies Inc.) and cloned into the pCAGGS expression vector. The plasmid (pCAG-SARS-CoV-2) containing a 19 aa truncation at the C-terminus of the spike protein was constructed. The pCAG-SARS-CoV-2 expression vector was transfected into 293T cells on collagen-coated tissue culture plates. After 24 h of incubation, the cells were infected with G-complemented VSVΔG/Luc[38] at a multiplicity of infection of 0.5, and thereafter, the uninfected viruses were washed. After 24 h of incubation, the culture supernatants with VSV pseudotyped virus were collected, centrifuged to remove cell debris, and then stored at -80 °C until use for the virus neutralization assay.

For the pseudotyped virus neutralization assay, SARS-CoV-2 pseudotyped virus was incubated with an equal volume of serially diluted, heat-inactivated plasma (five 5-fold serial dilutions starting at 1:10 dilution) for 1 h at 37 °C. The mixture was inoculated into VeroE6/TMPRSS2 cells (JCRB1819, JCRB Cell Bank) seeded in 96-well solid white flat-bottom plates (Corning), and then incubated for 24 h at 37 °C in a chamber supplied with 5% CO_2. VeroE6/TMPRSS2 cells were maintained in DMEM (Fujifilm Wako Pure Chemical) containing 10% heat-inactivated fetal bovine serum (FBS, Biowest), 1 mg/mL geneticin (Thermo Fisher Scientific), and 100 U/mL penicillin/streptomycin (Thermo Fisher Scientific). Luciferase activity in cultured cells was measured using the Bright-Glo Luciferase Assay System (Promega) with a

GroMax Navigator Microplate Luminometer (Promega). Half-maximal inhibitory concentration (IC_{50}) was calculated using Prism 9 (GraphPad) and presented as neutralization titers.

NT titers of COVID-19 convalescent patients were partially referred from a previous publication (Moriyama et. al. Immunity 2021, in Figure 1D). The criteria of data selection were the same as described in ELISA section.

Flow cytometry

For analysis of MDSCs, after blocking non-specific antibody binding using Human TruStain FcX (1:200, BioLegend) for 5 min at room temperature, cells were stained for 2 h at 4 °C with the following antibodies: CD45-APC-Alexa Fluor 700 (HIB30, 1:300; BD Biosciences), CD3-BV605 (SK7, 1:300, BD Biosciences), CD19-BV605 (HIB19, 1:300, BioLegend), CD56-BV605 (5.1H11, 1:300 BioLegend), HLA-DR-PE-Cy7 (G46-6, 1:300, BD Biosciences), CD11b-FITC (ICRF44, 1:300 BioLegend), CD33-PE (P67.6, 1:300 BioLegend), CD14-BV421 (M5E2, 1:300, BD Biosciences), and CD15-APC (W6D3, 1:300 BioLegend). To analyze the 15 immune cell types of interest, cryopreserved PBMCs were thawed at 37 °C and washed twice with RPMI 1640 (FUJIFILM Wako Pure Chemical Corporation) containing 10% heat-inactivated fetal bovine serum (Nichirei Biosciences), 2 mM glutamine (FUJIFILM Wako Pure Chemical Corporation), 100 U/mL penicillin (FUJIFILM Wako Pure Chemical Corporation), and 100 µg/mL streptomycin (FUJIFILM Wako Pure Chemical Corporation) before use. After blocking of non-specific antibody binding as described above, cells were stained for 2 hours at 4 °C with the following antibodies: CD45-BV570 (HI30, 1:150), CD3-BUV661 (HIT3a, 1:300, BD Biosciences), CD4-PE-Cy5.5 (RPA-T4, 1:100, BD Biosciences), CD8-BB660 (RPA-T8, 1:300, BD Biosciences), CD8-BV786 (RPA-T8, 1:300, BD Biosciences), CD19-BUV563 (SJ25C1, 1:300, BD Biosciences), CD56-BB515 (B159, 1:300, BD Biosciences), HLA-DR-APC-H7 (G46-6, 1:300, BD Biosciences), CD14-BV421 (M5E2, 1:300, BD Biosciences), CD16-BUV395 (3G8, 1:300, BD Biosciences), CD11c-APC-R700 (BU15, 1:300, BD Biosciences), CD88-PE-Cy7 (S5/1, 1:300 BioLegend), CD1c-BUV737 (F10/21A3, 1:300, BD Biosciences), CD123-BUV496 (6H6, 1:300, BD Biosciences), CD141-BV605 (1A4, 1:300, BD Biosciences), CD5-BV480 (UCHT2, 1:300, BD Biosciences), CD163-PE-CF594 (GHI/61, 1:300, BD Biosciences), CD163-BV786 (GHI/61, 1:300, BD Biosciences), Siglec-6-BV650 (767329, 1:300, BD Biosciences), Axl-BUV615 (108724, 1:300, BD Biosciences). After staining, the cells were washed twice and resuspended in PBS containing 0.5% BSA, 5 mM EDTA (Thermo Fisher Scientific), and 0.25 µg/mL 7-AAD (Sigma) to detect dead cells. MDSCs were analyzed using a FACS Canto II (BD Biosciences) or FACS Aria III cytometer (BD Biosciences) and FACS Diva v.9.0 software (BD Biosciences), and 15 immune cells other than MDSCs were analyzed using a FACS Symphony S6 cytometer (BD Biosciences) and FACS Diva v.9.0 software (BD Biosciences).

Flow cytometry data analysis

FCS files were analyzed using FlowJo software (v.10.8.0, BD Biosciences). Gating strategies for identifying immune cells are shown in Extended Data Fig. 2. The frequency of each immune cell population was calculated as a proportion of $CD45^+$ $7\text{-}AAD^-$ cells (live $CD45^+$ cells).

Cytokine / chemokine quantification

Plasma cytokines/chemokines were measured using a cytometric bead array kit (BD Biosciences) according to the manufacturer's instructions. Plasma samples were diluted 4-fold for analysis. Data were acquired using a FACS Canto II cytometer (BD Biosciences) and analyzed using FCAP Array Software Version 3.0 (BD Biosciences). For plasma cytokine levels below the detection limit, the value was set to 40 pg/mL.

Statistical analysis

Primary and secondary immune cell post/pre ratios were calculated as follows: primary, (cell frequency at day 1) / (cell frequency at day 0); secondary, (cell frequency at day 22) / (cell frequency at day 21). The cytokine/chemokine post/pre ratio was calculated as follows: (concentration at day 21) / (concentration at day 22). For generating Z-score for validating adverse event-related cellular parameters, each immune cell post/pre ratio was log-2 transformed, normalized to have a mean of 0 and a variance of 1. Composite scores were then calculated by directly summing these normalized values. All other parameters were analyzed without additional data transformation. Statistical analyses and visual representation were performed using Prism 9. (GraphPad).

RBD IgG, pseudotyped virus NT titer, local or systemic symptom severity scores, cytokine/chemokine post/pre ratios, age, and BMI were compared using the Kruskal-Wallis test followed by Dunn's post hoc test (Fig. 1b–d, 3b–e, 3 g –j) or Mann-Whitney test (Fig. 5b–c, 5e–g, Extended Data Fig. 1a–b).

Longitudinal analysis of local and systemic symptom severity scores (Fig. 1e) and plasma cytokine/chemokine concentrations (Extended Data Fig. 4) were performed using the Wilcoxon test. Fisher's exact test was performed to examine the statistical difference in the incidence of symptoms between primary and secondary vaccinations (Fig. 1f–g).

High-dimensional analysis was performed using the scikit-learn python library. Frequency data of 18 immune cell types at 4 time points (day 0, 1, 21, and 22) were standardized by removing the mean and scaling to unit variance, and dimensionality reduction to a two-dimensional space was performed using Uniform Manifold Approximation and Projection (UMAP) (Fig. 1j, Extended Data Fig. 4a–c).

Spearman correlations between primary and secondary symptom severity scores (Fig. 1h–i), cell post/pre ratios, antibody responses, symptom severity scores, and plasma cytokine/chemokine post/pre ratios (Fig. 2, Fig. 3a, Fig. 3f, Fig. 4, Extended Data Fig. 5) were identified. Correlations were considered significant at $p < 0.05$.

To validate the correlations between cellular parameters and adverse events or between cellular parameters and antibody responses, cellular parameters were stratified as follows: In cases that the cell post/pre ratios inversely correlated with adverse events or antibody responses, the cell post/pre ratios below the median of the cohort were identified as "positive", and vice versa for "negative". In Fig. 5 and

Extended Data Fig. 7, participants whose cellular parameters were all "positive" (all parameters were below the median of the cohort) were stratified as the matched group, and vice versa.

In all statistical analyses, significance was considered as follows: *p < 0.05, **p < 0.01, ***p < 0.001, and ****p < 0.0001.

Declarations

Acknowledgments

This work was supported by Japan Agency for Medical Research and Development grant (JP20fk0108534 to TM and YT). We thank Rutaro Iwabuchi, Akira Dosaka, Eriko Izumiyama, Emi Kohda, Rieko Iwaki, Tami Kobayashi, Chiyuki Asano, Naoka Yoshida for technical support; and Ryoko Itami for secretarial assistance.

Author Contributions

Conceptualization: T.M., Y.T.

Methodology: T.T., K.Tomii, K.Y., T.M.

Investigation: T.T., M.M., Y.A., K.K., N.S., S.M., L.S., M.I., A.N., T.O., K.Terahara, K.Tonouchi, M.N., K.Tomii, K.Y., T.M.

Funding acquisition: T.M., Y.T.

Project administration: K.K., T.M., M.S., Y.T.

Supervision: M.S., Y.T.

Writing—original draft: T.T., T.M., Y.T.

Writing—review & editing: T.T., Y.A., N.S., S.M., M.I., K.Terahara, K.Tomii, K.Y., T.M., Y.T.

Competing Interests statement

N.S. is an employee of KOTAI Biotechnologies, Inc. K.Y. is a founder, shareholder and board director of KOTAI Biotechnologies, Inc. The authors otherwise have no competing interest.

References

1. Polack, F.P., *et al.* Safety and efficacy of the BNT162b2 mRNA Covid-19 vaccine. *N Engl J Med* **383**, 2603–2615 (2020).
2. Moriyama, S., *et al.* Temporal maturation of neutralizing antibodies in COVID-19 convalescent individuals improves potency and breadth to circulating SARS-CoV-2 variants. *Immunity* **54**, 1841–

1852 e1844 (2021).

3. Modenese, A., *et al.* Neutralizing anti-SARS-CoV-2 antibody titer and reported adverse effects, in a sample of Italian nursing home personnel after two doses of the BNT162b2 vaccine administered four weeks apart. *Vaccines (Basel)* **9**, 652 (2021).
4. Michos, A., *et al.* Association of total and neutralizing SARS-CoV-2 spike -receptor binding domain antibodies with epidemiological and clinical characteristics after immunization with the 1(st) and 2(nd) doses of the BNT162b2 vaccine. *Vaccine*, in press (2021).
5. Coggins, S.A.A., *et al.* Adverse effects and antibody titers in response to the BNT162b2 mRNA COVID-19 vaccine in a prospective study of healthcare workers. *medRxiv*, https://doi.org/10.1101/2021.1106.1125.21259544 (2021).
6. Maeda, K., *et al.* Correlates of neutralizing/SARS-CoV-2-S1-binding antibody response with adverse effects and immune kinetics in BNT162b2-vaccinated individuals. *medRxiv*, https://doi.org/10.1101/2021.1107.1127.21261237 (2021).
7. Naaber, P., *et al.* Dynamics of antibody response to BNT162b2 vaccine after six months: a longitudinal prospective study. *Lancet Reg Health Eur*, 100208 (2021).
8. Menni, C., *et al.* Vaccine side-effects and SARS-CoV-2 infection after vaccination in users of the COVID Symptom Study app in the UK: a prospective observational study. *Lancet Infect Dis* **21**, 939–949 (2021).
9. Goel, R.R., *et al.* Distinct antibody and memory B cell responses in SARS-CoV-2 naive and recovered individuals following mRNA vaccination. *Sci Immunol* **6**, eabi6950 (2021).
10. Knudson, C.J., *et al.* Lipid-nanoparticle-encapsulated mRNA vaccines induce protective memory CD8 T cells against a lethal viral infection. *Mol Ther* **29**, 2769–2781 (2021).
11. Sahin, U., *et al.* BNT162b2 vaccine induces neutralizing antibodies and poly-specific T cells in humans. *Nature* **595**, 572–577 (2021).
12. Painter, M.M., *et al.* Rapid induction of antigen-specific CD4(+) T cells is associated with coordinated humoral and cellular immunity to SARS-CoV-2 mRNA vaccination. *Immunity* **54**, 2133–2142 e2133 (2021).
13. Goel, R.R., *et al.* mRNA vaccination induces durable immune memory to SARS-CoV-2 with continued evolution to variants of concern. *bioRxiv*, https://www.biorxiv.org/content/10.1101/2021.1108.1123.457229v457221 (2021).
14. Arunachalam, P.S., *et al.* Systems vaccinology of the BNT162b2 mRNA vaccine in humans. *Nature* **596**, 410–416 (2021).
15. Wimmers, F., *et al.* The single-cell epigenomic and transcriptional landscape of immunity to influenza vaccination. *Cell* **184**, 3915–3935 e3921 (2021).
16. Gaya, M., *et al.* Initiation of antiviral B cell immunity relies on innate signals from spatially positioned NKT cells. *Cell* **172**, 517–533 e520 (2018).

17. Zingaropoli, M.A., *et al.* Major reduction of NKT cells in patients with severe COVID-19 pneumonia. *Clin Immunol* **222**, 108630 (2021).
18. Nakaya, H.I., *et al.* Systems analysis of immunity to influenza vaccination across multiple years and in diverse populations reveals shared molecular signatures. *Immunity* **43**, 1186–1198 (2015).
19. Pellini, R., *et al.* Initial observations on age, gender, BMI and hypertension in antibody responses to SARS-CoV-2 BNT162b2 vaccine. *EClinicalMedicine* **36**, 100928 (2021).
20. Lustig, Y., *et al.* BNT162b2 COVID-19 vaccine and correlates of humoral immune responses and dynamics: a prospective, single-centre, longitudinal cohort study in health-care workers. *Lancet Respir Med* **9**, 999–1009 (2021).
21. Cagigi, A. & Lore, K. Immune responses induced by mRNA vaccination in mice, monkeys and humans. *Vaccines (Basel)* **9**, 61 (2021).
22. Liang, F., *et al.* Efficient targeting and activation of antigen-presenting cells In vivo after modified mRNA vaccine administration in rhesus macaques. *Mol Ther* **25**, 2635–2647 (2017).
23. Bourdely, P., *et al.* Transcriptional and functional analysis of CD1c(+) human dendritic cells identifies a CD163(+) subset priming CD8(+)CD103(+) T cells. *Immunity* **53**, 335–352 e338 (2020).
24. Cytlak, U., *et al.* Differential IRF8 transcription factor requirement defines two pathways of dendritic cell development in humans. *Immunity* **53**, 353–370 e358 (2020).
25. Dutertre, C.A., *et al.* Single-cell analysis of human mononuclear phagocytes reveals subset-defining markers and identifies circulating inflammatory dendritic cells. *Immunity* **51**, 573–589 e578 (2019).
26. Alcantara-Hernandez, M., *et al.* High-dimensional phenotypic mapping of human dendritic cells reveals interindividual variation and tissue specialization. *Immunity* **47**, 1037–1050 e1036 (2017).
27. Leylek, R., *et al.* Integrated cross-species analysis identifies a conserved transitional dendritic cell population. *Cell Rep* **29**, 3736–3750 e3738 (2019).
28. See, P., *et al.* Mapping the human DC lineage through the integration of high-dimensional techniques. *Science* **356**, eaag3009 (2017).
29. Villani, A.C., *et al.* Single-cell RNA-seq reveals new types of human blood dendritic cells, monocytes, and progenitors. *Science* **356**, eaah4573 (2017).
30. Manetti, R., *et al.* Natural killer cell stimulatory factor (interleukin 12 [IL-12]) induces T helper type 1 (Th1)-specific immune responses and inhibits the development of IL-4-producing Th cells. *J Exp Med* **177**, 1199–1204 (1993).
31. Hsieh, C.S., *et al.* Development of TH1 CD4 + T cells through IL-12 produced by Listeria-induced macrophages. *Science* **260**, 547–549 (1993).
32. Harrington, L.E., *et al.* Interleukin 17-producing CD4 + effector T cells develop via a lineage distinct from the T helper type 1 and 2 lineages. *Nat Immunol* **6**, 1123–1132 (2005).
33. Revu, S., *et al.* IL-23 and IL-1beta drive human Th17 cell differentiation and metabolic reprogramming in absence of CD28 costimulation. *Cell Rep* **22**, 2642–2653 (2018).

34. Morales-Nunez, J.J., *et al.* Neutralizing antibodies titers and side effects in response to BNT162b2 vaccine in healthcare workers with and without prior SARS-CoV-2 Infection. *Vaccines (Basel)* **9**, 742 (2021).
35. Adachi, Y., *et al.* Exposure of an occluded hemagglutinin epitope drives selection of a class of cross-protective influenza antibodies. *Nat Commun* **10**, 3883 (2019).
36. Tiller, T., *et al.* Efficient generation of monoclonal antibodies from single human B cells by single cell RT-PCR and expression vector cloning. *J Immunol Methods* **329**, 112–124 (2008).
37. Tani, H., *et al.* Evaluation of SARS-CoV-2 neutralizing antibodies using a vesicular stomatitis virus possessing SARS-CoV-2 spike protein. *Virol J* **18**, 16 (2021).
38. Tani, H., *et al.* Involvement of ceramide in the propagation of Japanese encephalitis virus. *J Virol* **84**, 2798–2807 (2010).

Figures

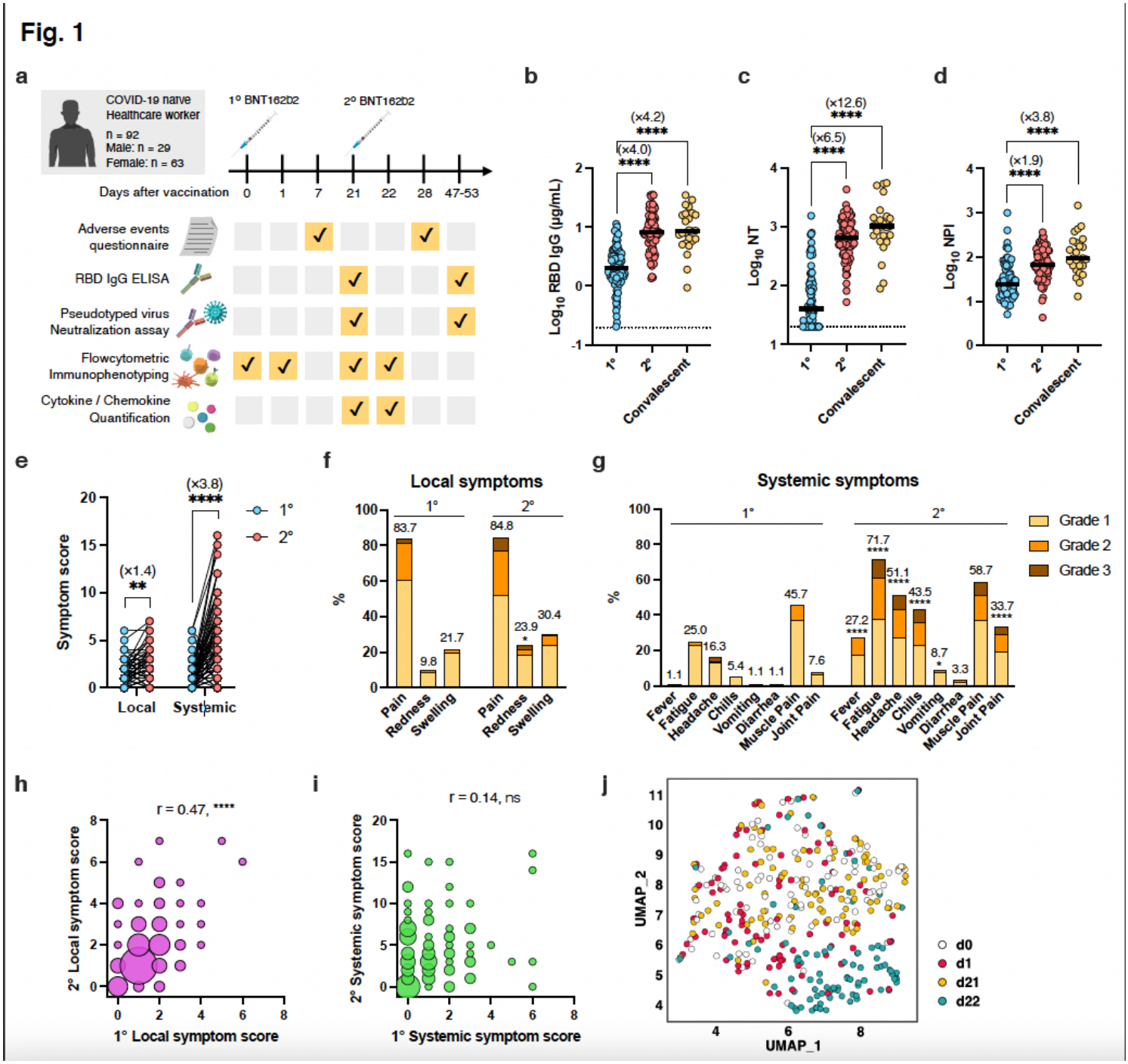

Figure 1

BNT162b2 elicits antibody responses, adverse reactions, and distinct cell dynamics. a, A cohort of healthcare workers with two vaccinations of BNT162b2 (n = 92) was evaluated for antibody responses, incidents of adverse events, dynamics of immune cells among PBMCs, and cytokine/chemokine production. b–d, Antibody responses elicited by vaccination. b, RBD IgG. c, Pseudotyped virus NT titers. d, NPI. 1° (day 21), n = 92; 2° (day 47–53), n = 92; COVID-19 convalescent: n = 25. The bars represent the median values. Kruskal-Wallis test: *p < 0.05, **p < 0.01, ***p < 0.001, ****p < 0.0001. Dashed lines, cut-off determined by ROC analysis. e, Total symptom severity score for local and systemic symptoms. Circles connected with a line represent data from the same individual. Wilcoxon test: **p < 0.01, ****p <

0.0001. f, g, Frequencies and severity of local (f) and systemic (g) adverse events; 1°, n = 92; 2°, n = 92. Fisher's exact test: *p < 0.05, **p < 0.01, ****p < 0.0001. h, i, Correlations between primary and secondary symptom severity scores of local (h) or systemic (i) symptoms after each vaccination. The sizes of the circles indicate the number of individuals. n = 92. Spearman's rank-order correlation coefficient test: ****p < 0.0001. j, UMAP of 18 immune cell frequencies. Data points for individual participants and colored by time point.

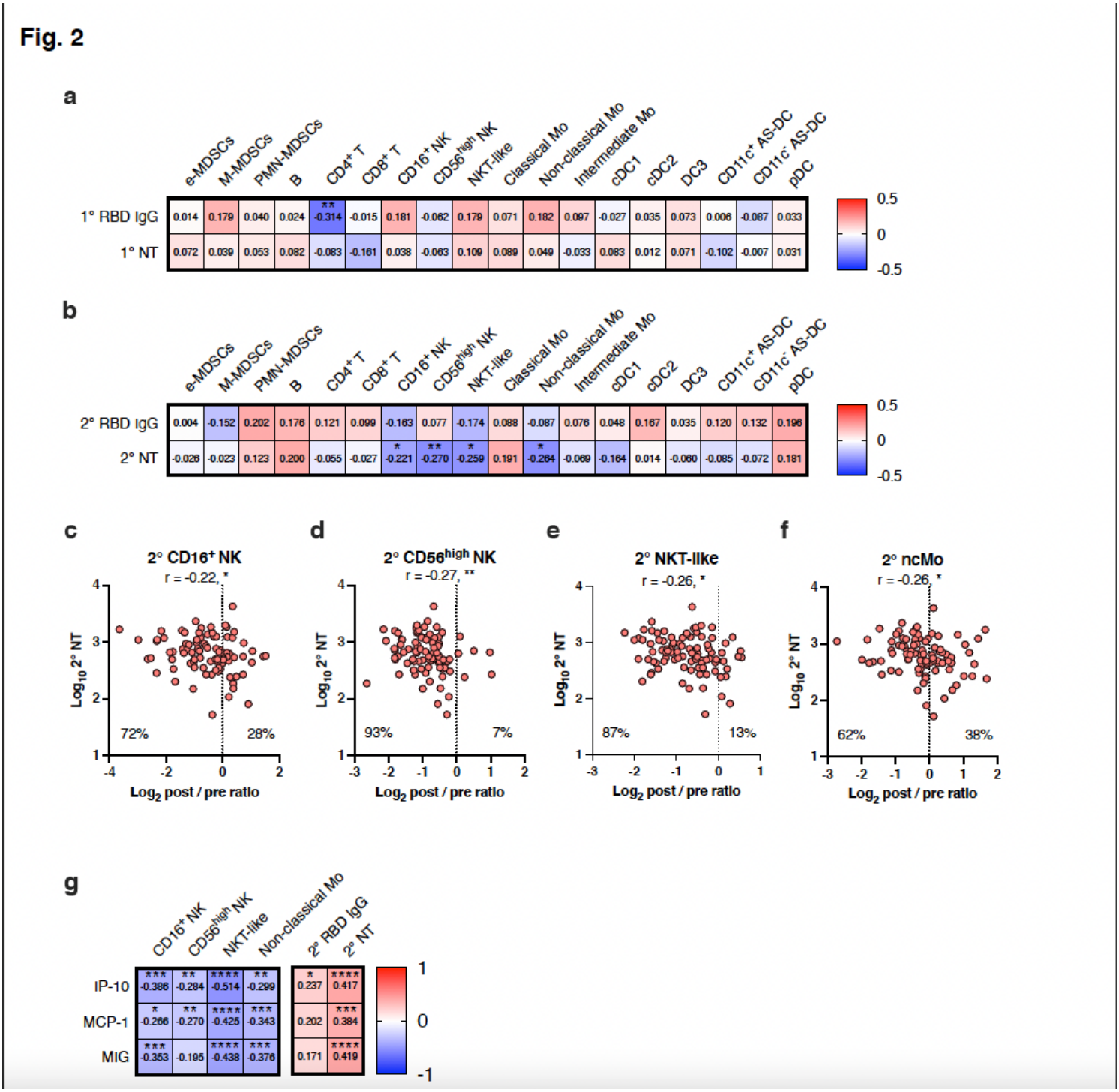

Figure 2

Early dynamics of NK and monocyte subsets link to neutralizing antibody response. a, b, Correlations between 18 immune cell dynamics and antibody responses. a, Cell dynamics (d1–d0 post/pre ratios), and antibody responses after primary vaccination. b, Cell dynamics (d22–d21 post/pre ratios) and antibody responses after secondary vaccination. Spearman's r values are indicated in each cell. c–f, Correlation plots between NT titer and cell dynamics (d22–d21 post/pre ratios). c, CD16+ NK cells. d, CD56high NK cells. e, NKT-like cells. f, Non-classical monocytes. g, Correlations between cytokine dynamics and cell dynamics (d22–d21 post/pre ratios) and antibody responses. Spearman's r values are indicated in each cell. Spearman's rank-order correlation coefficient test: *p < 0.05, **p < 0.01, ***p < 0.001, ****p < 0.0001.

Fig. 3

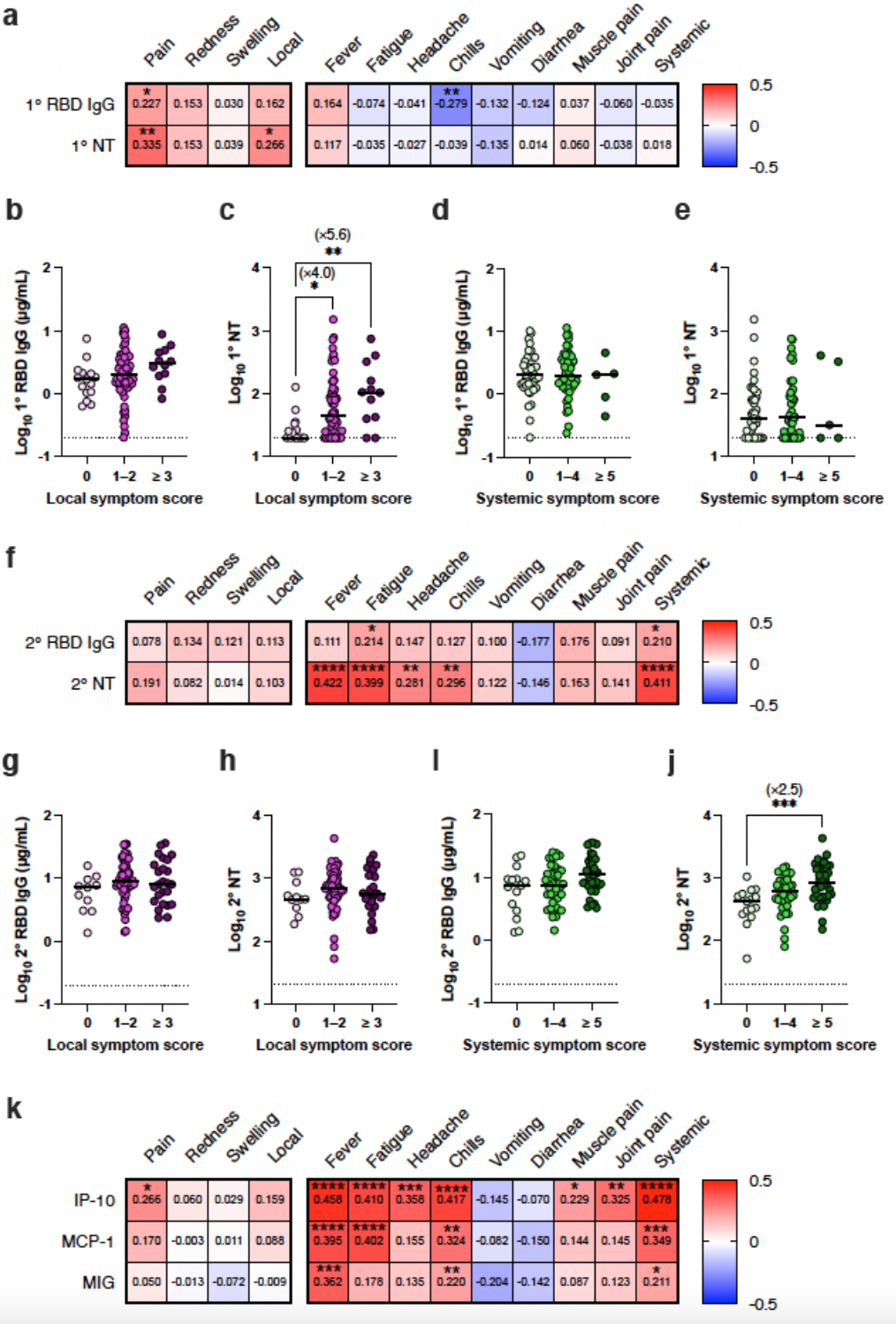

Figure 3

Adverse events correlate with neutralizing antibodies. a, Correlations between symptom severity scores and antibody responses. Spearman's r values are indicated in each cell. b, c, Antibody responses. b, RBD IgG. c, NT titers. 0, n = 15; 1–2, n = 65; ≥ 3, n = 12. Bars represent the median values. Kruskal-Wallis test: *p < 0.05, **p < 0.01. d, e, Antibody responses. d, RBD IgG. e, NT titers. 0, n = 40; 1–4, n = 47; ≥ 5, n = 5. Bars represent the median values. Kruskal-Wallis test. f, Correlations between symptom severity scores

and antibody responses. Spearman's r values are indicated in each cell. g, h, Antibody responses. g, RBD IgG. h, NT titers. 0, n = 11; 1–2, n = 56; ≥ 3, n = 25. RBD IgG titer. Bars represent the median values. i, j, Antibody responses. i, RBD IgG. j, NT titers. 0, n = 15; 1–4, n = 39; ≥ 5, n = 38. Bars represent the median values. Kruskal-Wallis test: ***p < 0.001. Kruskal-Wallis test: *p < 0.05, **p < 0.01. k, Correlations between cytokine dynamics and symptom severity scores. Spearman's r values are indicated in each cell. Spearman's rank-order correlation coefficient test: *p < 0.05, **p < 0.01, ***p < 0.001, ****p < 0.0001.

Fig. 4

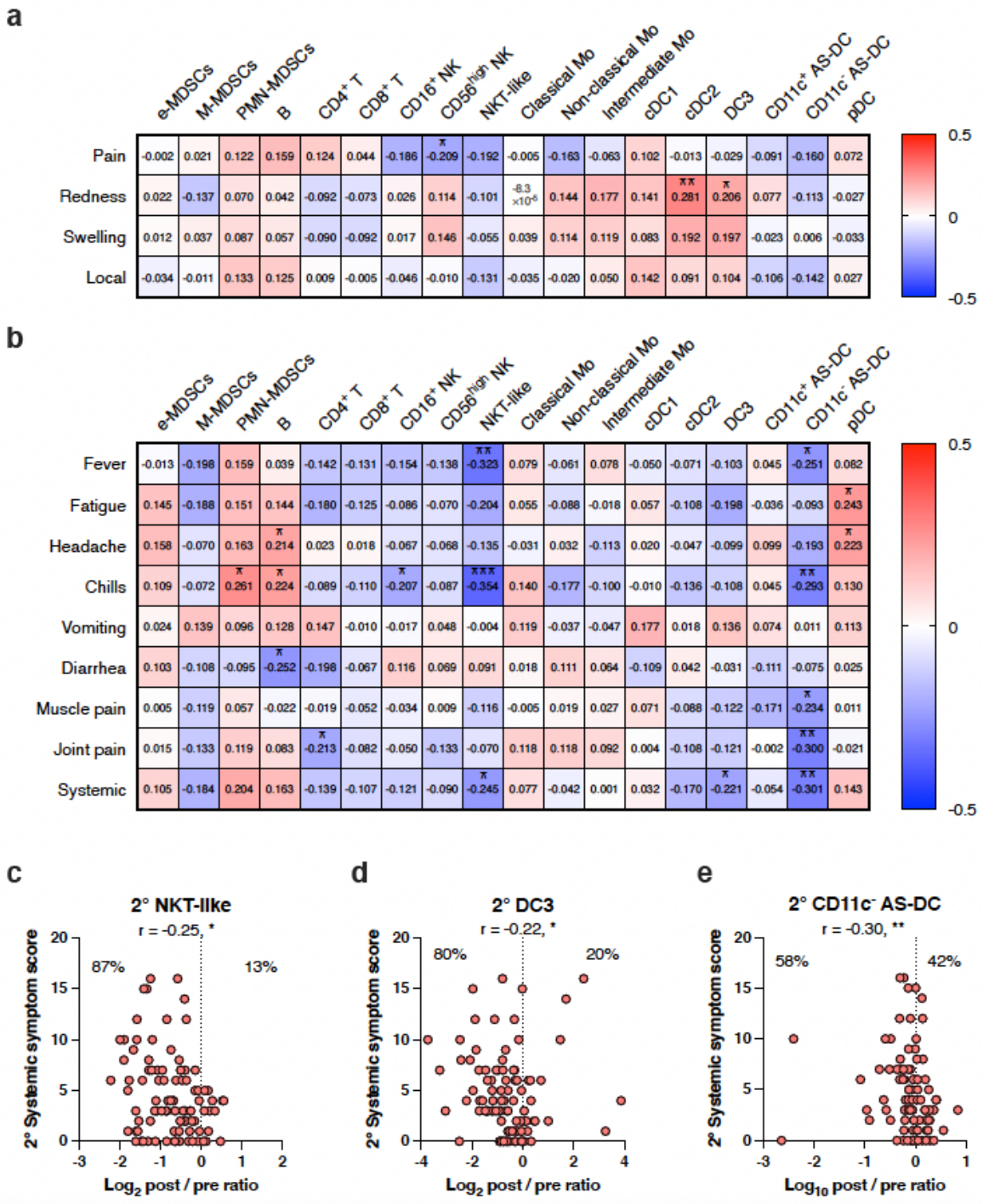

Figure 4

Early dynamics of NK and DC subsets link to adverse events. a, b, Correlations between symptom severity scores and cell dynamics. a, Local symptom severity scores on the second vaccination and cell dynamics. b, Systemic symptom severity scores on the second vaccination and cell dynamics. Spearman's r values are indicated in each cell. n = 92. c–e, Correlation plots between systemic symptom severity scores and cell dynamics (d22–d21 post/pre ratios). c, NKT-like cells. d, DC3s. e, CD11c- AS-DCs. Spearman's r values are indicated in each cell. n = 92. Spearman's rank-order correlation coefficient test: *p < 0.05, **p < 0.01, and ***p < 0.001.

Fig. 5

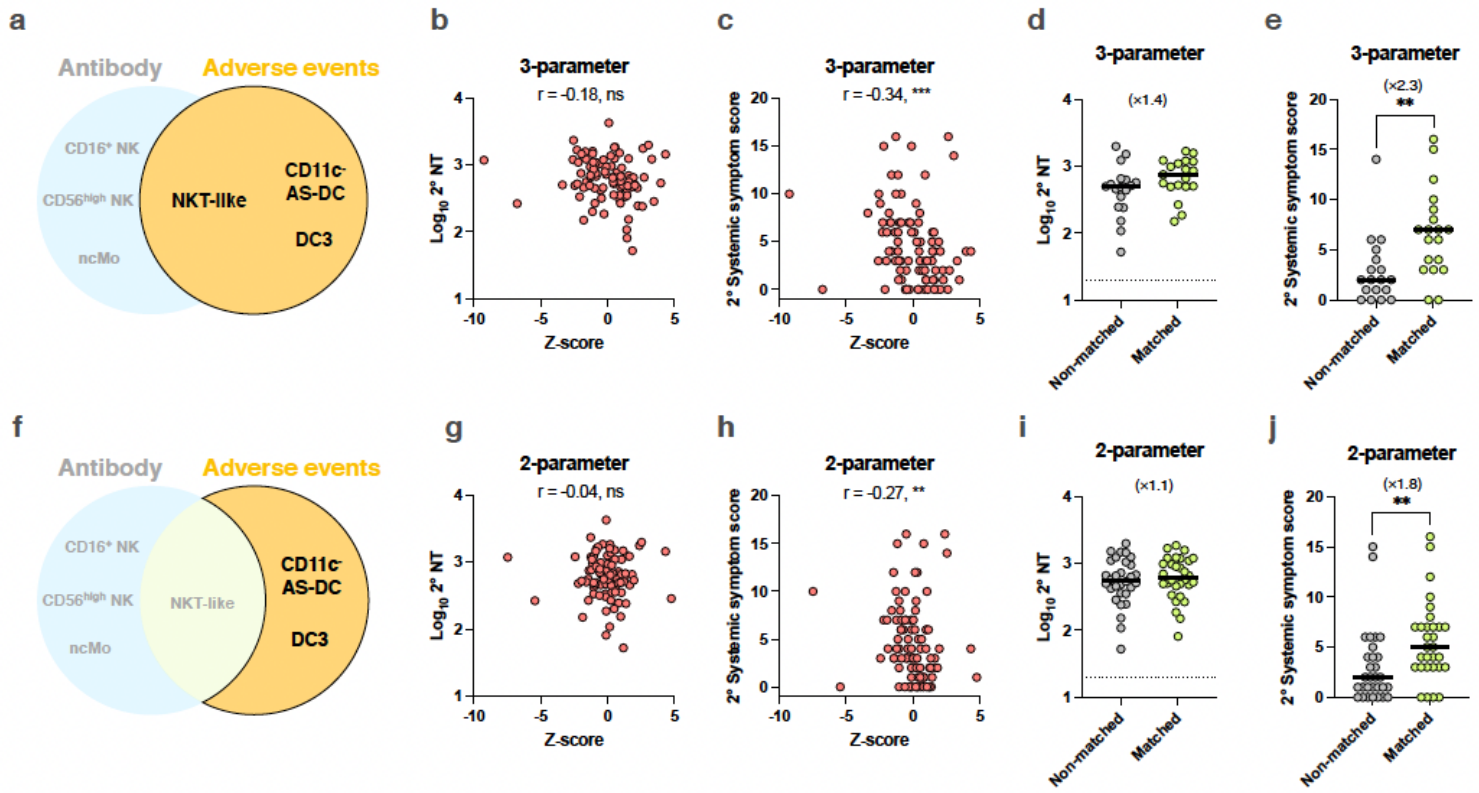

Figure 5

The combination of DC subset dynamics specifically associates with systemic symptom severity. a, Scheme of the 3-parameter model related to adverse events. b, c, Z-score was calculated based on 3 parameters (i.e., the post/pre ratios of NKT-like cells, DC3s, and CD11c- AS-DCs calculated as described in the Methods) and tested for correlation with NT (b) and systemic symptom severity score (c). n = 92. Spearman's rank-order correlation coefficient test: ***p < 0.001. d, e, Participants were stratified into matched group and non-matched group for the 3-parameter model related to adverse events. The matched group represents subjects positive for all 3 parameters, while the non-matched group represents subjects negative for all 3 parameters. d, NT titers. e, Systemic symptom severity scores. Matched group, n = 19; non-matched group, n = 18. Bars represent the median values. Mann-Whitney test: *p < 0.05, ****p < 0.0001. f, Scheme of the 2-parameter model specific to adverse events. g, h, Z-score was calculated based on 2 parameters (i.e., the post/pre ratios of DC3s and CD11c- AS-DCs) and tested for correlation

with NT (g) and systemic symptom severity score (h). Spearman's rank-order correlation coefficient test: **p < 0.01. i, j, Participants were stratified into matched and non-matched group for 2-parameter model specific to adverse events. i, NT titers. j, Systemic symptom severity scores. Matched group, n = 30; non-matched group, n = 30. Bars represent the median values. Mann-Whitney test: **p < 0.01.

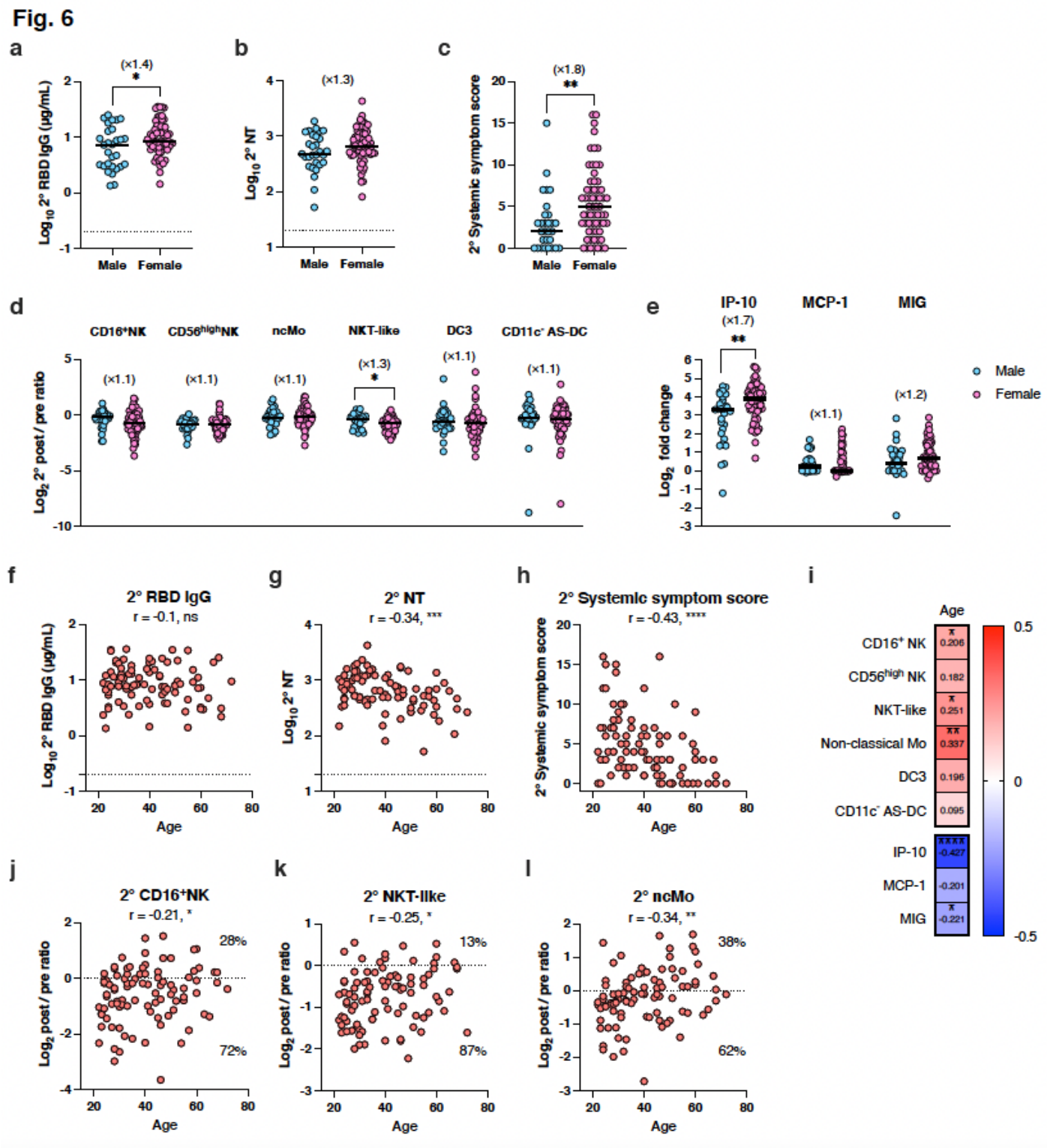

Figure 6

NK and monocyte subsets dynamics explain sex and age differences in antibody responses and adverse events. a, RBD IgG. b, NT titer. c, Systemic symptom severity scores. d, Cell dynamics (d22–d21 post/pre ratios). e, Cytokine dynamics (d22–d21 post/pre ratios). Male, n = 29; Female, n = 63. Bars represent the median values. Mann-Whitney test: *p < 0.05, **p < 0.01. f–h, Correlation plots between age and RBD IgG (f), NT (g), and systemic symptom severity scores (h). Spearman's rank-order correlation coefficient test: ***p < 0.001, ****p < 0.0001. n = 92. i, Correlations between age, cell dynamics, and cytokine dynamics. Spearman's r values are indicated in each cell. n = 92. Spearman's rank-order correlation coefficient test: *p < 0.05, **p < 0.01, ****p < 0.0001. j–l, Correlation plots between age and CD16+ NK cells (j), NKT-like cells (k), and non-classical monocytes (l). Spearman's rank-order correlation coefficient test: *p < 0.05, **p < 0.01. n = 92.

Supplementary Files

This is a list of supplementary files associated with this preprint. Click to download.

- SupplementalInformationS1Takanoetal210916.pdf
- 210917FigureTakanov4ExtendedDataFigure.pdf